1

2

3 **DNA damage-induced phosphorylation of histone H2A at serine 15 is linked to**

4 **DNA end resection**

5

6

7 Salar Ahmad and Jacques Côté#

8

9

10 St-Patrick Research Group in Basic Oncology, Centre Hospitalier Universitaire de Québec-

11 Université Laval Research Center, Laval University Cancer Research Center, Quebec City, QC,

12 Canada

13

14

15 **Running Title:** Phosphorylation of H2AS15 at DNA breaks

16

17

18 # Corresponding authors: jacques.cote@crhdq.ulaval.ca

19

20 **Word Count**

21 Introduction, Results and Discussion: 2,614

22 Materials and Methods: 1,005

23 **ABSTRACT**

24 The repair of DNA double-strand breaks (DSBs) occurs in chromatin and several histone post-
25 translational modifications have been implicated in the process. Modifications of histone H2A N-
26 terminal tail has also been linked to DNA damage response, through acetylation or ubiquitination
27 of lysine residues that regulate repair pathway choice. Here, we characterize a new DNA damage-
28 induced phosphorylation event on chromatin, at serine 15 of H2A in yeast. We show that this SQ
29 motif functions independently of the classical S129 C-terminal site (γH2A) and mutant mimicking
30 constitutive phosphorylation increases cell sensitivity to DNA damage. H2AS129ph is induced by
31 both Tel1^{ATM} and Mec1^{ATR}, and loss of Lcd1^{ATRIP} or Mec1 signaling decreases γH2A spreading distal
32 to DSB. In contrast, H2AS15ph is completely dependent on Lcd1^{ATRIP}, indicating that this
33 modification only happens when end resection is engaged. This link is supported by an increase
34 of RPA binding in the H2AS15E phosphomimic mutant, reflecting higher resection. This serine on
35 H2A is replaced by a lysine in higher eukaryotes (H2AK15), which undergoes an acetyl-
36 monoubiquityl switch to regulate binding of 53BP1 and therefore resection. This regulation
37 seems functionally conserved with budding yeast H2AS15 and the 53BP1-homolog Rad9, utilizing
38 different post-translational modifications between organisms but achieving the same function.

39

40

41 **INTRODUCTION**

42 The genetic information of the cell is challenged by various endogenous and exogenous cues
43 which leads to DNA damage. If unchecked this can lead to mutations, translocations, loss of
44 genetic information and in higher eukaryotes be the underlying cause for diseases such as cancer
45 (1, 2). One of the most harmful form of DNA damage is DNA double strand break (DSB). To endure
46 and mitigate such damage to the DNA, cells orchestrate cell cycle arrest and DNA repair
47 pathways, collectively termed DNA damage response (DDR). Two main pathways to repair DSBs
48 are non-homologous end joining (NHEJ) and homologous recombination (HR). NHEJ involves
49 direct ligation of the two broken DNA ends which may require processing, thus making it a more
50 error prone pathway (3). In HR, single stranded DNA (ssDNA) is generated through a process
51 called resection and involves use of homologous sequence or sister chromatid as a template to
52 copy the genetic information, thus ensuring a lower error rate (4).

53 Phosphatidylinositol-3-OH kinase related kinases (PIKKs) family has been implicated to
54 play an important role in DDR. This includes *S. cerevisiae* Tel1 and Mec1 and the mammalian
55 ataxia telangiectasia-mutated (ATM), AT-related (ATR) and DNA-dependent protein kinase (DNA-
56 PK) (5, 6). One of the first DNA damage-dependent chromatin modification to be identified was
57 γ-H2A(X), which is the phosphorylation of histone H2A at S129 in yeast and H2A.X at S139 in
58 mammals (7-9). This phosphorylation is carried out by both Tel1/ATM and Mec1/ATR. In yeast
59 H2AS129ph spreads more than 50Kb on both sides flanking the DSB, whereas in mammals it
60 spreads up to a megabase (10, 11). This histone mark has been implicated in DNA damage
61 response and required for proper recruitment of chromatin remodelers/modifiers such as Ino80,
62 Swr1 and NuA4 complexes (12-15). Mice model for $H2AX^{-/-}$ is radiation sensitive, growth retarded,

63 immune deficient and show recruitment defect for variety of repair factors such as Nbs1, 53BP1
64 and BRCA1 (16).

65 Interestingly, budding yeast has another Tel1/Mec1-dependent SQ phosphorylation site
66 at H2B C-terminus, H2BT129ph, which largely correlates with H2AS129ph but is modulated by it
67 (10). Other DNA damage-induced phosphorylation marks have been mapped on chromatin but
68 are not deposited by PIKKs. These include H4S1ph, H2AS122ph and H2AT126ph in yeast which
69 have been linked to processes like chromatin restoration after repair, meiosis, HR and repair of
70 fragile sites with CAG/CTG repeats (17-21). Apart from phosphorylation, other histone
71 modifications like acetylation, methylation, ubiquitylation and SUMOylation have been
72 implicated in DDR (22). In mammals H2AK15 is ubiquitinated by RNF168 and this mark is
73 responsible for recruitment and repair foci formation of 53BP1 in combination with H4K20me2,
74 inhibiting resection and favoring NHEJ (23). At DSBs, the TIP60 complex can acetylate H2AK15
75 and binds H4K20me, thus antagonizing 53BP1 and favoring repair by HR (24). In budding yeast,
76 Rad9 is the functional homolog of 53BP1, contains a Tudor domain which binds H3K79me
77 (equivalent to mammalian H4K20) and a BRCT domain which recognizes γ-H2A (25-27). Both of
78 these domains are required for the recruitment and retention of Rad9 at DSBs (27, 28). In
79 contrast to 53BP1, Rad9 does not have a ubiquitin-binding domain neither the yeast H2A has
80 lysine corresponding to human H2AK15 (Fig. 1A). Instead, yeast H2A has a SQ site at this position
81 which has been found phosphorylated in a Mec1-dependent manner upon DNA damage, in a
82 large phosphoproteomic study (29).

83 This led us to investigate whether H2AS15 had a role in the repair of DNA breaks. Our
84 results indicate that H2AS15ph is induced by $Mec1^{ATR}$ over a large domain of chromatin around

85 the DSB. We also present data arguing that H2AS15ph regulates Rad9 binding and DNA end
86 resection. Altogether these results suggest an evolutionary conserved mechanism, similar to the
87 mammalian H2AK15 ubiquitin/acetylation switch, in modulating yeast Rad9^{53BP1} binding in
88 response to DSB repair.
89
90 **RESULTS**
91 **H2AS15ph function is distinct from H2AS129ph in response to DNA damage**
92 In order to investigate if H2A-S15 has a role in DNA damage response, we mutated H2A-S15 to
93 alanine (non-phosphorylation mimicking) and glutamic acid (phosphorylation mimicking). In
94 presence of DNA damaging agent methyl methanesulfonate (MMS), *H2A-S15E* mutant cells show
95 a slight growth defect which is not seen for *H2A-S15A* (Fig. 1B). However, in combination with
96 the *H2A-S129A* mutant, both *H2A-S15A/E* show stronger growth defect compared to single *H2A-*
97 *S129A* mutant cells (Fig. 1B). Next, we tested if the *H2A-S15* mutants had any genetic interaction
98 with the other PIKK-dependent histone phosphorylation induced in response to DSBs in yeast,
99 H2BT129ph (10). *H2A-S15A/E H2B-T129A* double mutant cells do not show any additional growth
100 defect compared to *H2A-S15* single mutants in presence of MMS (Fig. 1C). These results indicate
101 that H2AS129 and H2AS15 phosphorylations play distinct roles in response to DNA damage
102 induced by MMS.
103 To decipher if *H2A-S15* mutants affects H2AS129 phosphorylation *in vivo*, we performed
104 ChIP-qPCR at an inducible DSB. We used the yeast background in which a single persistent DNA
105 double strand break is created at the *MAT* locus by homothallic endonuclease (HO) inducible by
106 galactose. The induced H2AS129ph signal detected on each side of the DSB in wild type (WT)

107 background corresponds to what was previously reported (10, 12). Both *H2A-S15A/E* mutants
108 show similar pattern of H2AS129ph compared to WT cells, not affecting the induction or
109 spreading of H2A-S129ph beside a very small increase in the *H2A-S15E* mutant (Fig. 1D-E). These
110 results again support a role of H2AS15ph in DNA damage response/repair that is distinct of
111 H2AS129ph.

112 The lysine residues of H2A and H4 N-terminal tails are known targets of the NuA4
113 acetyltransferase complex (30). Studies have described histone modifications modulating the
114 occurrence of other modifications in chromatin, thus forming a network of histone crosstalk (22).
115 H4S1ph carried out by CK2 has been shown to inhibit acetylation of various lysine residues on
116 the N-terminal tail of H4 and play an active role in DSB repair as well as transcription (17, 18).
117 This raised the question whether H2AS15ph could influence acetylation of lysine residues on the
118 H2A and H4 N-terminal tails. Western blot analysis of whole cell extracts from yeast cells
119 harboring the *H2A-S15* point mutants reveals a small decrease in both H2A and H4 acetylation
120 more noticeable for the *H2A-S15A* mutant compared to wild type (Fig. 1F). We further
121 investigated *in vivo* if the *H2A-S15* mutants affected the acetylation of histones around DSB. Both
122 *H2A-S15A/E* mutants show a decrease in H4 acetylation signal but only close to the DNA break
123 site (Fig. 1G). These results suggest that H2AS15ph has a small but significant effect on other
124 histone modifications in regions surrounding the DSB.

125

126 **H2AS15ph is induced over a large chromatin domain upon DNA double strand break formation**

127 To characterize the dynamics of H2AS15ph in response to DNA damage, we produced and
128 purified an antibody against the *S. cerevisiae* H2A N-terminal portion with Ser15 bearing the

129 phosphorylation mark. To demonstrate that H2AS15ph is indeed regulated by DNA damage, we
130 performed immunoblotting with purified yeast native chromatin. As shown in (Fig. 2A),
131 H2AS15ph signal increases with MMS treatment, similarly to H2AS129ph. A control using
132 phosphatase treatment of the chromatin confirms that the signal detected by the antibody is
133 indeed phosphorylation-specific (Fig. 2B).

134 To determine whether H2AS15ph occurs at the DSB, we performed ChIP-qPCR after
135 induction at the *MAT* locus. The signal detected for H2AS15ph shows a clear increase around the
136 DSB site in WT background spanning over 10 kilobases on each side of the break (Fig. 2C). As a
137 control to check the specificity of the signal detected, the *H2A-S15A* mutant cells do not show
138 such signal over a large domain after the induction of DSB (Fig. 2C). However, close to the break
139 site, *H2A-S15A* mutant cells do show a slight increase which likely reflects some non-specific
140 cross-reactivity of the antibody with another mark. To characterize the dynamics of H2AS15ph
141 appearance around the DSB, the ChIP-qPCRs were performed at different time-points after
142 induction of the break. Interestingly, appearance of H2AS15ph seems delayed in comparison to
143 H2AS129ph, reaching maximum levels throughout the region after 3hrs (Fig. 2D-E). Altogether,
144 these data clearly demonstrate that H2AS15ph is actively deposited over a large region of
145 chromatin upon formation of DNA double strand breaks.

146

147 **Mec1^{ATR} and not Tel1^{ATM} phosphorylates H2AS15 at DSBs**

148 Tel1^{ATM} and Mec1^{ATR} signaling kinases phosphorylate histone H2AS129 to form γ-H2A (7, 11, 31).
149 They also target various proteins to modulate DSB repair and checkpoint activation. Recruitment
150 of Tel1 to DSB requires Xrs2 (mammalian NBS1), subunit of the Mre11-Rad50-Xrs2 (MRX)

151 complex (32). Deletion of *XRS2* affects Tel1 dependent checkpoint signaling and telomere
152 maintenance functions (33). Yeast Lcd1/Ddc2 (mammalian ATRIP) is responsible for the
153 recruitment of Mec1 to RPA-coated single stranded DNA (ssDNA) produced during end resection
154 (34). Mec1 has been shown to be involved in spreading of γ-H2A in *trans* onto adjacent
155 undamaged chromosomes in close physical proximity (10, 35). Deletion of *LCD1* is known to incur
156 loss of Mec1 recruitment to RPA-coated ssDNA and therefore Mec1-dependent cell signaling in
157 response to damage (36, 37).

158 *lcd1*Δ and *lcd1*Δ*xrs2*Δ mutant cells lead respectively to loss of Mec1 and both Mec1 and
159 Tel1 at the DSB. In *lcd1*Δ, where Tel1 recruitment and signaling is unaffected, ChIP-qPCR
160 experiments show that the signal for γ-H2A is similar to WT close to the break (Fig. 3A). However,
161 farther from the break, at 7Kb and 10Kb, the signal is significantly reduced, showing its relation
162 to Mec1. In *lcd1*Δ*xrs2*Δ, both Mec1 and Tel1 recruitments being abrogated, the γ-H2A signal is
163 completely abolished (Fig. 3A). This is similar to what is observed for *mec1*Δ and *mec1*Δ*tel1*Δ
164 mutant cells in previous studies (10). Loss of *MEC1* affects γ-H2A spreading away from the break
165 site, whereas loss of *MEC1* and *TEL1* results in complete loss of γ-H2A.

166 A large scale phosphoproteomic study has detected phosphorylation of H2AS15 and
167 linked it to Mec1 (29). To investigate this, we carried out ChIP-qPCR using the H2AS15ph antibody
168 to study its spreading around the DSB in *lcd1*Δ and *lcd1*Δ*xrs2*Δ mutant cells. As shown above,
169 wild type cells show enrichment for H2A-S15ph over a large region on each side of the DSB (Fig.
170 3B). However, *lcd1*Δ as well as *lcd1*Δ*xrs2*Δ mutant cells do not show any H2AS15ph signal.
171 Overall, the above data demonstrate that, unlike γ-H2A which is brought about by the kinase

172 activity of Mec1 and Tel1, H2AS15ph is carried out solely by Mec1 and is therefore linked to
173 resection after DSB formation.
174
175 **H2AS15 is required to maintain fidelity of resection**
176 Previously studies have shown that the *H2A-S129A* non-phosphorylation mutant leads to faster
177 resection from the HO-induced DSB compared to wild type cells (38, 39). This increased resection
178 may be attributed to the inability of Rad9 to bind H2AS129ph. Yeast Rad9 like its mammalian
179 homolog 53BP1 functions in slowing down or keeping a check on end resection rate (40-43). To
180 investigate whether H2AS15ph may affect resection, we used an antibody against Rfa1 (RPA
181 largest subunit) as a proxy for the ssDNA generated by resection in ChIP-qPCR at the HO-induced
182 DSB. Interestingly, *H2A-S15E* (phosphorylation mimicking) mutant cells show increased
183 resection, whereas *H2A-S15A* mutant cells behave like wild type (Fig. 4A). The double mutants
184 *H2A-S15A/E H2AS129A* have similar increased resection patterns as *H2A-S129A* cells, maybe
185 slightly less than *H2AS15E* cells (Fig. 4A). An interesting possibility is whether H2AS15ph is also
186 recognized by the BRCT domain of Rad9, this domain being well characterized for its ability to
187 bind H2AS129ph (26). Surprisingly, *in vitro* peptide binding assays with recombinant Rad9
188 indicate a clear binding preference for the histone H2A tail peptide, but in its non-phosphorylated
189 form (Fig. 4B). Importantly, this binding is also confirmed using yeast whole cell extracts in
190 peptide pull-downs and detecting endogenous Rad9 by immunoblotting (Fig. 4C). In this case,
191 inducing DNA damage in the cells does not affect endogenous Rad9 ability to bind the H2A
192 peptide *in vitro*. This ability of H2AS15ph to block Rad9 binding to the H2A histone tail may in
193 part explain the increased end resection detected in *H2A-S15E* mutant cells but not in *H2A-S15A*

194 (Fig. 4A). Altogether, these results implicate the DNA damage-induced H2AS15ph histone mark
195 in the end resection fidelity at DSBs.
196
197 **DISCUSSION**
198 Histone tails are sites of various post-translational modifications (PTMs) such as phosphorylation,
199 acetylation, methylation, ubiquitylation and SUMOylation. These modifications are recognized
200 by reader proteins containing specialized domains such as ubiquitin binding domains, BRCT and
201 FHA domains which bind phosphorylation, Chromodomains, MBT domains, Bromodomains and
202 PHD fingers which recognize methylation or acetylation. Proteins and protein complexes use
203 these interactions for their proper recruitment, retention and orientation at the target sites to
204 carry out their respective functions (44, 45).
205 In this study, we characterized yeast H2AS15ph as a novel histone modification in the
206 context of DNA damage. This modification is induced in presence of DNA damaging agent MMS,
207 which is a known alkylating agent and produces DSBs as cells replicate their DNA in S-phase. A
208 large-scale proteomic study had identified H2AS15ph by mass spectrometry and implicated
209 $Mec1^{ATR}$ for its detection (29). Using *in vivo* analysis, we show that indeed Mec1, and not Tel1, is
210 responsible for the induction of this mark around DNA breaks, unlike γ-H2A (H2AS129ph) which
211 is brought about by either Tel1 or Mec1 (Fig. 3). While the spreading of γ-H2A at DSB is not
212 affected in *H2A-S15A/E* mutant cells, a decrease of chromatin acetylation is detected in close
213 proximity to the DSB (Fig. 1). We know from previous studies that acetylation of histone H4 and
214 H2A by the NuA4 complex plays an important role for the recruitment of various chromatin

215 remodelers like INO80, RSC and SWI/ SNF required for repair by HR (12, 46, 47). Future work will
216 be needed to determine if H2AS15 affects the recruitment of these remodelers.

217 A most interesting finding reported here argues that yeast H2AS15ph corresponds to an
218 evolutionary conserved regulatory function to regulate 53BP1/Rad9 binding to the H2A tail and
219 DNA end resection, consequently DSB repair pathway choice. The yeast H2AS15 residue seems
220 the functional homolog of mammalian H2AK15 in modulating resection which in turn affects DNA
221 repair pathway selection, albeit through different PTMs. In mammals, when 53BP1 binds
222 H2AK15ub in the vicinity of DSBs, it inhibits resection and favors the NHEJ pathway. This binding
223 in turn inhibits TIP60-mediated acetylation of H2AK15 which otherwise would block
224 ubiquitylation by RNF168 and 53BP1 binding, favoring resection and HR (24). *H2A-S15E* mutant
225 cells show increased resection, as seen with *H2A-S129A* mutant cells where Rad9^{53BP1} is incapable
226 to bind and inhibit or slow down resection (Fig. 4A). *In vitro* data suggest that Rad9 binds the H2A
227 N-terminal tail in its unmodified state and this binding is abolished when H2AS15 is
228 phosphorylated (Fig. 4B-C). We proposed a model depicted in (Fig. 4D) where resection of DNA
229 ends produces ssDNA which gets coated by RPA and recruits Mec1^{ATR} through its binding partner
230 Lcd1/Ddc2^{ATRIP} (34, 36). Mec1 then phosphorylates H2AS15 which inhibits Rad9 binding and
231 therefore increases resection. H2AS15ph may be a dynamic mark, switching between
232 phosphorylation and non-phosphorylation states to fine-tune the process of resection. This
233 conserved function of the H2A tail to regulate Rad9/53BP1 binding and resection is even further
234 supported by a recent report showing phosphorylation of the ubiquitin moiety of H2AK15ub
235 (H2AK15pUbT12) to inhibit 53BP1 binding and favor resection (48).

236 Future work will address whether specific proteins may bind H2AS15ph. While our
237 peptide pull-downs with yeast extracts followed by mass spectrometry did not yield clear results
238 (data not shown), we speculate that other DNA repair proteins such as Rtt107 and Dpb11 which
239 have BRCT domains could recognize H2AS15ph. Rtt107 was recently shown to bind H4T80ph and
240 γ-H2A to counteract Rad9-modulated checkpoint activity (49). Dpb11 has been shown to act as a
241 scaffold protein for various checkpoint proteins and is involved in Rad9 recruitment/retention at
242 DSBs (50, 51). H2AS15 may also act redundantly with other DNA damage induced histone
243 phosphorylation marks and function as a scaffold for proper orientation or retention of repair
244 factors.
245

246 **MATERIAL AND METHODS**

247 **Yeast strains**

248 All yeast strains used in the current study are from FY-406 (52) and JKM-179 (53) (*hta1-*
249 *htb1Δ::NatMX* , *hta2-htb2Δ::KANMX*) background carrying deletion of both copies of H2A and
250 H2B genes. These strains carry an ectopic copy of *HTA1-HTB1* on a low copy vector pRS413 (in
251 FY-406) and pRS414 (in JKM-179). Gene deletion and point mutations were obtained through
252 standard PCR techniques. Plasmid shuffling using 5-Fluoroorotic acid (5-FOA) was employed to
253 introduce the plasmid with point mutations in respective backgrounds. Yeast background
254 JKM139 (53) containing deletion of *sml1Δ::NATMX* , *lcd1Δ::KANMX* , *xrs2Δ::TRP1* was used in
255 this study. QY-362 (JKM139 *RAD9-13MYC::KANMX*) was also used in this study for peptide pull
256 down experiment. General lithium acetate method was used to transform the yeast cells. Cells
257 were grown in YPD (1% yeast extract, 2% peptone, 2% dextrose) at 30°C till early log phase. For
258 spot assay 1:10 dilution of the culture was spotted and grown at 30°C for 3-4 days.

259 **Chromatin Immunoprecipitation (ChIP)**

260 ChIP-qPCR was performed as described previously (54). In brief, cells were grown overnight in
261 YP-Raffinose till OD600 was 0.5-1, at this point galactose (2%) was added to induced DSB at *MAT*
262 locus for 3 hours. This was followed by cross-linking of cells with formaldehyde and lysing with
263 bead-beater. Sonication was performed on Diagenode Bioruptor to obtain chromatin size of
264 ~200-500bp. 100μg of chromatin was used to setup the immunoprecipitation reaction with anti-
265 H2A-S129ph (Upstate 07-745), anti-H2A-S15Ph (antibody was produced in rabbit using the
266 peptide sequence: Ac-GSAAKA(pS)QSRSAK-C. Affinity purification was performed to improve the
267 specificity of the antibody. Antibody was produced by Thermo Fisher Scientific), anti-Rfa1

268 (Agrisera AS07214), anti-H4ac (Upstate 06-946) and anti-H4 (Abcam 7311) and reaction was
269 allowed to mix on a wheel overnight at 4°C. Next morning Protein-A agarose beads were added
270 followed by additional 3-4 hours on a wheel at 4°C. After multiple washing steps the DNA was
271 eluted and incubated at 65°C overnight for de-cross linking followed by phenol-chloroform
272 extraction of DNA. This DNA was resuspended in NTE and used for qPCR. LC480 LightCycler
273 (Roche) was used to quantify DNA with the primer pairs as mentioned in the respective figures
274 to calculate % of immunoprecipitation (IP)/ input. The data represents mean of two independent
275 biological replicates. Error bars indicate the ranges between the two biological replicates. Fold
276 enrichment represents ratio of %IP/input at indicated loci around DSB normalized on signal at
277 negative-control locus IntergenicV. Primer sequences are available upon request.

278 **Purification of native yeast chromatin**

279 Native yeast chromatin was prepared as described previously (55), cells were treated with MMS
280 (0.05%) or DMSO (control) for 2 hours to induce DNA damage. Lambda protein phosphatase
281 (λPP) (NEB) kit was used. The reaction mixture was incubated for 30 mins at 30°C followed by
282 booster of λPP and additional incubation for 30 mins at 30°C.

283 **Recombinant protein purification**

284 Recombinant Rad9 (C-terminal containing Tudor and BRCT domains) protein was purified as
285 described previously (56). In short, bacterial cells were grown overnight at 16°C with IPTG
286 induction. Next day cells were lysed with lysozyme followed by sonication. The soluble portion
287 was incubated with glutathione sepharose (GE healthcare) beads for 3-4 hours at 4°C and eluted
288 with glutathione. The eluted protein concentration was quantified by running on SDS-PAGE with
289 known BSA standards followed by coomassie staining.

290 **Peptide-pull down**

291 Peptide-pull down was performed with synthetic peptide corresponding to H2A N-terminal (aa
292 1-23) obtained from AnaSpec. 1μg of peptide was incubated with 1μg of GST-tagged protein
293 overnight on wheel at 4°C in binding buffer (50 mM Tris–HCl pH 7.5, 50 mM NaCl, 0.1% NP-40, 1
294 mM PMSF and phosphatase inhibitors). Next morning streptavidin dynabeads was added to the
295 reaction mixture and kept at 4°C for two additional hours followed by washing, running on SDS-
296 PAGE and western blotting with anti-GST (Sigma G1160).

297 Peptide-pull down with yeast cell extract was performed by growing cells in YPD and treating
298 with MMS (0.05%) or DMSO for 2 hours till OD_{600} ~1.0-1.5. Cells were centrifuged and pellet was
299 wash with cold mQ. Pellet was resuspended in sensitization buffer (100mM Tris-HCl pH 9.4,
300 10mM DTT) and incubated at 30°C on a wheel for 15 mins. Centrifuged at 500g for 5mins at 4°C
301 and resuspended in 30ml of spheroplasting buffer (1.2M Sorbitol 20mM Hepes pH 7.5).
302 Centrifuged and resuspended again in 40ml of spheroplasting buffer with lyticase, incubated on
303 wheel at 30°C for one and half hour. Centrifuged at 500g for 5 mins and washed with wash buffer
304 (1.2M Sorbitol, 20mM Pipes pH 6.4, 1mM $MgCl_2$) and resuspended in 25ml of nuclear isolation
305 buffer; NIB (250mM Sucrose, 60mM KCl, 1mM PMSF, 14mM NaCl, 0.8% Triton X-100, 5mM
306 $MgCl_2$, 1mM $CaCl_2$, 15mM MES) mixed well to remove clumps and kept on ice for 20 mins.
307 Centrifuged and washed two times with NIB till white nuclear pellet was obtained. Resuspended
308 in pull-down buffer (400mM NaCl, 1mM PMSF, 50mM Tris-HCl pH8, 0.5% NP-40, 5 mM β-
309 glycerophosphate, 10 mM sodium butyrate, 5 mM NaF) to get 300mM NaCl in final volume and
310 kept on rotating plate at 4°C for 20 mins. Centrifuged at 14,000rpm at 4°C for 30 mins and
311 collected the supernatant (nuclear extract). Biotinylated peptides were bound to streptavidin

312 dynabeads in peptide binding buffer (150mM NaCl, 50mM Tris-HCl pH8.0, 0.1% NP-40, 5 mM β-
313 glycerophosphate, 10 mM sodium butyrate, 5 mM NaF) by incubating at room temperature on
314 wheel for 30 mins. Peptide-dynabeads were washed with protein binding buffer (140mM NaCl,
315 50mM Tris-HCl pH 8.0, 0.1% NP-40, 0.5mM DTT, 10μM $ZnCl_2$, 5 mM β-glycerophosphate, 10 mM
316 sodium butyrate, 5 mM NaF) followed by addition of 600ug of nuclear extract to each pull-down
317 reaction and incubated at 4°C on wheel for 2 hours. Nuclear extract that was incubated with
318 phospho peptide was initially incubated with non-phospho peptide, on the other hand, nuclear
319 extract for non-phospho peptide was initially incubated with phospho peptide for 2 hours at 4°C
320 on wheel. Washed 3-4 times with final wash buffer (350mM NaCl, 50mM Tris-HCl pH8.0, 0.1%
321 NP-40, 0.5mM DTT, 10μM $ZnCl_2$, 5 mM β-glycerophosphate, 10 mM sodium butyrate, 5 mM NaF)
322 followed by addition of laemmli buffer, boiled and resolved in SDS-PAGE followed by western
323 blotting with anti-Myc (9E10 Babco MMS150R).
324
325 ***Acknowledgments***
326 We thank Xue Cheng for important advice and Valérie Côté for technical support. We are grateful
327 to Jim Haber for sharing reagents/strains and stimulating discussions. This work was supported
328 by a grant from the Canadian Institutes of Health Research (CIHR) to J.C. (FDN-143314). S.A. held
329 a Desjardins/Fondation du CHU de Québec studentship. J.C. holds the Canada Research Chair in
330 Chromatin Biology and Molecular Epigenetics.
331
332
333 **REFERENCES**

334 1. Hanahan D, Weinberg RA. 2011. Hallmarks of cancer: the next generation. Cell 144:646-
335 74.
336 2. Jackson SP, Bartek J. 2009. The DNA-damage response in human biology and disease.
337 Nature 461:1071-8.
338 3. Chiruvella KK, Liang Z, Wilson TE. 2013. Repair of double-strand breaks by end joining.
339 Cold Spring Harb Perspect Biol 5:a012757.
340 4. Symington LS. 2016. Mechanism and regulation of DNA end resection in eukaryotes. Crit
341 Rev Biochem Mol Biol 51:195-212.
342 5. Abraham RT. 2001. Cell cycle checkpoint signaling through the ATM and ATR kinases.
343 Genes Dev 15:2177-96.
344 6. Smith GC, Jackson SP. 1999. The DNA-dependent protein kinase. Genes & development
345 13:916-934.
346 7. Downs JA, Lowndes NF, Jackson SP. 2000. A role for Saccharomyces cerevisiae histone
347 H2A in DNA repair. Nature 408:1001-1004.
348 8. Paull TT, Rogakou EP, Yamazaki V, Kirchgessner CU, Gellert M, Bonner WM. 2000. A critical
349 role for histone H2AX in recruitment of repair factors to nuclear foci after DNA damage.
350 Current Biology 10:886-895.
351 9. Rogakou EP, Boon C, Redon C, Bonner WM. 1999. Megabase Chromatin Domains Involved
352 in DNA Double-Strand Breaks in Vivo. The Journal of Cell Biology 146:905-916.
353 10. Lee CS, Lee K, Legube G, Haber JE. 2014. Dynamics of yeast histone H2A and H2B
354 phosphorylation in response to a double-strand break. Nat Struct Mol Biol 21:103-9.

355 11. Shroff R, Arbel-Eden A, Pilch D, Ira G, Bonner WM, Petrini JH, Haber JE, Lichten M. 2004.
356 Distribution and dynamics of chromatin modification induced by a defined DNA double-
357 strand break. Curr Biol 14:1703-11.
358 12. Downs JA, Allard S, Jobin-Robitaille O, Javaheri A, Auger A, Bouchard N, Kron SJ, Jackson
359 SP, Côté J. 2004. Binding of Chromatin-Modifying Activities to Phosphorylated Histone
360 H2A at DNA Damage Sites. Molecular Cell 16:979-990.
361 13. Morrison AJ, Highland J, Krogan NJ, Arbel-Eden A, Greenblatt JF, Haber JE, Shen X. 2004.
362 INO80 and gamma-H2AX interaction links ATP-dependent chromatin remodeling to DNA
363 damage repair. Cell 119:767-75.
364 14. van Attikum H, Fritsch O, Gasser SM. 2007. Distinct roles for SWR1 and INO80 chromatin
365 remodeling complexes at chromosomal double-strand breaks. EMBO J 26:4113-25.
366 15. van Attikum H, Fritsch O, Hohn B, Gasser SM. 2004. Recruitment of the INO80 complex by
367 H2A phosphorylation links ATP-dependent chromatin remodeling with DNA double-
368 strand break repair. Cell 119:777-88.
369 16. Celeste A, Petersen S, Romanienko PJ, Fernandez-Capetillo O, Chen HT, Sedelnikova OA,
370 Reina-San-Martin B, Coppola V, Meffre E, Difilippantonio MJ, Redon C, Pilch DR, Olaru A,
371 Eckhaus M, Camerini-Otero RD, Tessarollo L, Livak F, Manova K, Bonner WM,
372 Nussenzweig MC, Nussenzweig A. 2002. Genomic Instability in Mice Lacking Histone
373 H2AX. Science 296:922-927.
374 17. Cheung WL, Turner FB, Krishnamoorthy T, Wolner B, Ahn SH, Foley M, Dorsey JA, Peterson
375 CL, Berger SL, Allis CD. 2005. Phosphorylation of histone H4 serine 1 during DNA damage
376 requires casein kinase II in S. cerevisiae. Curr Biol 15:656-60.

377 18. Utley RT, Lacoste N, Jobin-Robitaille O, Allard S, Cote J. 2005. Regulation of NuA4 histone
378 acetyltransferase activity in transcription and DNA repair by phosphorylation of histone
379 H4. Mol Cell Biol 25:8179-90.
380 19. Harvey AC, Jackson SP, Downs JA. 2005. Saccharomyces cerevisiae histone H2A Ser122
381 facilitates DNA repair. Genetics 170:543-53.
382 20. Krishnamoorthy T, Chen X, Govin J, Cheung WL, Dorsey J, Schindler K, Winter E, Allis CD,
383 Guacci V, Khochbin S, Fuller MT, Berger SL. 2006. Phosphorylation of histone H4 Ser1
384 regulates sporulation in yeast and is conserved in fly and mouse spermatogenesis. Genes
385 & development 20:2580-2592.
386 21. House NCM, Polleys EJ, Quasem I, De la Rosa Mejia M, Joyce CE, Takacsi-Nagy O, Krebs JE,
387 Fuchs SM, Freudenreich CH. 2019. Distinct roles for S. cerevisiae H2A copies in
388 recombination and repeat stability, with a role for H2A.1 threonine 126. eLife 8:e53362.
389 22. Dantuma NP, van Attikum H. 2016. Spatiotemporal regulation of posttranslational
390 modifications in the DNA damage response. The EMBO Journal 35:6-23.
391 23. Fradet-Turcotte A, Canny MD, Escribano-Díaz C, Orthwein A, Leung CC, Huang H, Landry
392 MC, Kitevski-LeBlanc J, Noordermeer SM, Sicheri F, Durocher D. 2013. 53BP1 is a reader
393 of the DNA-damage-induced H2A Lys 15 ubiquitin mark. Nature 499:50-4.
394 24. Jacquet K, Fradet-Turcotte A, Avvakumov N, Lambert JP, Roques C, Pandita RK, Paquet E,
395 Herst P, Gingras AC, Pandita TK, Legube G, Doyon Y, Durocher D, Côté J. 2016. The TIP60
396 Complex Regulates Bivalent Chromatin Recognition by 53BP1 through Direct H4K20me
397 Binding and H2AK15 Acetylation. Mol Cell 62:409-421.

398 25. Grenon M, Costelloe T, Jimeno S, O'Shaughnessy A, FitzGerald J, Zgheib O, Degerth L,
399 Lowndes NF. 2007. Docking onto chromatin via the Saccharomyces cerevisiae Rad9 Tudor
400 domain. Yeast 24:105-119.
401 26. Hammet A, Magill C, Heierhorst J, Jackson SP. 2007. Rad9 BRCT domain interaction with
402 phosphorylated H2AX regulates the G1 checkpoint in budding yeast. EMBO Rep 8:851-7.
403 27. Wysocki R, Javaheri A, Allard S, Sha F, Côté J, Kron SJ. 2005. Role of Dot1-Dependent
404 Histone H3 Methylation in G₁ and S Phase DNA Damage Checkpoint
405 Functions of Rad9. Molecular and Cellular Biology 25:8430-8443.
406 28. Javaheri A, Wysocki R, Jobin-Robitaille O, Altaf M, Cote J, Kron SJ. 2006. Yeast G1 DNA
407 damage checkpoint regulation by H2A phosphorylation is independent of chromatin
408 remodeling. Proc Natl Acad Sci U S A 103:13771-6.
409 29. Bastos de Oliveira FM, Kim D, Cussiol JR, Das J, Jeong MC, Doerfler L, Schmidt KH, Yu H,
410 Smolka MB. 2015. Phosphoproteomics reveals distinct modes of Mec1/ATR signaling
411 during DNA replication. Mol Cell 57:1124-1132.
412 30. Allard S, Utley RT, Savard J, Clarke A, Grant P, Brandl CJ, Pillus L, Workman JL, Côté J. 1999.
413 NuA4, an essential transcription adaptor/histone H4 acetyltransferase complex
414 containing Esa1p and the ATM-related cofactor Tra1p. The EMBO Journal 18:5108-5119.
415 31. Redon C, Pilch DR, Rogakou EP, Orr AH, Lowndes NF, Bonner WM. 2003. Yeast histone 2A
416 serine 129 is essential for the efficient repair of checkpoint-blind DNA damage. EMBO
417 reports 4:678-684.
418 32. Nakada D, Matsumoto K, Sugimoto K. 2003. ATM-related Tel1 associates with double-
419 strand breaks through an Xrs2-dependent mechanism. Genes Dev 17:1957-62.

420 33. Oh J, Al-Zain A, Cannavo E, Cejka P, Symington LS. 2016. Xrs2 Dependent and Independent
421 Functions of the Mre11-Rad50 Complex. Mol Cell 64:405-415.
422 34. Zou L, Elledge SJ. 2003. Sensing DNA Damage Through ATRIP Recognition of RPA-ssDNA
423 Complexes. Science 300:1542-1548.
424 35. Li K, Bronk G, Kondev J, Haber JE. 2020. Yeast ATM and ATR kinases use different
425 mechanisms to spread histone H2A phosphorylation around a DNA double-strand break.
426 Proceedings of the National Academy of Sciences 117:21354-21363.
427 36. Gobbini E, Cesena D, Galbiati A, Lockhart A, Longhese MP. 2013. Interplays between
428 ATM/Tel1 and ATR/Mec1 in sensing and signaling DNA double-strand breaks. DNA Repair
429 (Amst) 12:791-9.
430 37. Paciotti V, Clerici M, Lucchini G, Longhese MP. 2000. The checkpoint protein Ddc2,
431 functionally related to S. pombe Rad26, interacts with Mec1 and is regulated by Mec1-
432 dependent phosphorylation in budding yeast. Genes & Development 14:2046-2059.
433 38. Chen X, Cui D, Papusha A, Zhang X, Chu CD, Tang J, Chen K, Pan X, Ira G. 2012. The Fun30
434 nucleosome remodeller promotes resection of DNA double-strand break ends. Nature
435 489:576-80.
436 39. Eapen VV, Sugawara N, Tsabar M, Wu WH, Haber JE. 2012. The Saccharomyces cerevisiae
437 chromatin remodeler Fun30 regulates DNA end resection and checkpoint deactivation.
438 Mol Cell Biol 32:4727-40.
439 40. Ferrari M, Dibitetto D, De Gregorio G, Eapen VV, Rawal CC, Lazzaro F, Tsabar M, Marini F,
440 Haber JE, Pellicioli A. 2015. Functional interplay between the 53BP1-ortholog Rad9 and

441 the Mre11 complex regulates resection, end-tethering and repair of a double-strand
442 break. PLoS Genet 11:e1004928.
443 41. Escribano-Díaz C, Orthwein A, Fradet-Turcotte A, Xing M, Young JT, Tkáč J, Cook MA,
444 Rosebrock AP, Munro M, Canny MD, Xu D, Durocher D. 2013. A cell cycle-dependent
445 regulatory circuit composed of 53BP1-RIF1 and BRCA1-CtIP controls DNA repair pathway
446 choice. Mol Cell 49:872-83.
447 42. Noordermeer SM, Adam S, Setiaputra D, Barazas M, Pettitt SJ, Ling AK, Olivieri M, Alvarez-
448 Quilon A, Moatti N, Zimmermann M, Annunziato S, Krastev DB, Song F, Brandsma I,
449 Frankum J, Brough R, Sherker A, Landry S, Szilard RK, Munro MM, McEwan A, Goullet de
450 Rugy T, Lin ZY, Hart T, Moffat J, Gingras AC, Martin A, van Attikum H, Jonkers J, Lord CJ,
451 Rottenberg S, Durocher D. 2018. The shieldin complex mediates 53BP1-dependent DNA
452 repair. Nature 560:117-121.
453 43. Zimmermann M, Lottersberger F, Buonomo SB, Sfeir A, de Lange T. 2013. 53BP1 Regulates
454 DSB Repair Using Rif1 to Control 5' End Resection. Science 339:700-704.
455 44. Wilson MD, Durocher D. 2017. Reading chromatin signatures after DNA double-strand
456 breaks. Philos Trans R Soc Lond B Biol Sci 372.
457 45. Rossetto D, Truman AW, Kron SJ, Cote J. 2010. Epigenetic modifications in double-strand
458 break DNA damage signaling and repair. Clin Cancer Res 16:4543-52.
459 46. Bennett G, Peterson CL. 2015. SWI/SNF recruitment to a DNA double-strand break by the
460 NuA4 and Gcn5 histone acetyltransferases. DNA Repair 30:38-45.

461 47. House NCM, Yang JH, Walsh SC, Moy JM, Freudenreich CH. 2014. NuA4 initiates dynamic
462 histone H4 acetylation to promote high-fidelity sister chromatid recombination at
463 postreplication gaps. Mol Cell 55:818-828.
464 48. Walser F, Mulder MPC, Bragantini B, Burger S, Gubser T, Gatti M, Botuyan MV, Villa A,
465 Altmeyer M, Neri D, Ovaa H, Mer G, Penengo L. 2020. Ubiquitin Phosphorylation at Thr12
466 Modulates the DNA Damage Response. Molecular Cell 80:423-436.e9.
467 49. Millan-Zambrano G, Santos-Rosa H, Puddu F, Robson SC, Jackson SP, Kouzarides T. 2018.
468 Phosphorylation of Histone H4T80 Triggers DNA Damage Checkpoint Recovery. Mol Cell
469 72:625-635 e4.
470 50. Liu Y, Cussiol JR, Dibitetto D, Sims JR, Twayana S, Weiss RS, Freire R, Marini F, Pellicioli A,
471 Smolka MB. 2017. TOPBP1(Dpb11) plays a conserved role in homologous recombination
472 DNA repair through the coordinated recruitment of 53BP1(Rad9). J Cell Biol 216:623-639.
473 51. Granata M, Lazzaro F, Novarina D, Panigada D, Puddu F, Abreu CM, Kumar R, Grenon M,
474 Lowndes NF, Plevani P, Muzi-Falconi M. 2010. Dynamics of Rad9 chromatin binding and
475 checkpoint function are mediated by its dimerization and are cell cycle-regulated by CDK1
476 activity. PLoS Genet 6.
477 52. Hirschhorn JN, Bortvin AL, Ricupero-Hovasse SL, Winston F. 1995. A new class of histone
478 H2A mutations in Saccharomyces cerevisiae causes specific transcriptional defects in vivo.
479 Molecular and Cellular Biology 15:1999-2009.
480 53. Lee SE, Moore JK, Holmes A, Umezu K, Kolodner RD, Haber JE. 1998.
481 Saccharomyces Ku70, Mre11/Rad50, and RPA Proteins Regulate Adaptation
482 to G2/M Arrest after DNA Damage. Cell 94:399-409.

483 54. Rossetto D, Cramet M, Wang AY, Steunou AL, Lacoste N, Schulze JM, Cote V, Monnet-
484 Saksouk J, Piquet S, Nourani A, Kobor MS, Cote J. 2014. Eaf5/7/3 form a functionally
485 independent NuA4 submodule linked to RNA polymerase II-coupled nucleosome
486 recycling. EMBO J 33:1397-415.
487 55. Altaf M, Utley RT, Lacoste N, Tan S, Briggs SD, Cote J. 2007. Interplay of chromatin
488 modifiers on a short basic patch of histone H4 tail defines the boundary of telomeric
489 heterochromatin. Mol Cell 28:1002-14.
490 56. Setiaputra D, Ahmad S, Dalwadi U, Steunou A-L, Lu S, Ross JD, Dong M-Q, Côté J, Yip CK.
491 2018. Molecular Architecture of the Essential Yeast Histone Acetyltransferase Complex
492 NuA4 Redefines Its Multimodularity. Molecular and Cellular Biology 38:e00570-17.
493
494

495 **FIGURE LEGENDS**

496 **Fig 1: *H2A-S15* mutants are sensitive to DNA damage and functions independently of γ-H2A.**

497 (A) Sequence of H2A N-termini highlighting the SQ site at position 15 in *S. cerevisiae* and
498 corresponding lysine at position 15 in *H. sapiens*.

499 (B, C) Phenotypic analysis of yeast cells expressing wild type or the indicated H2A mutants. Ten-
500 fold serial dilutions of log phase cells were spotted on plates containing rich media alone or in
501 presence of DNA damaging agent methylmethane sulfonate (MMS). *H2A-S15E* showed a slight
502 growth defect in presence of the drug. Whereas, both *H2A-S15A/E* in background with *H2A-*
503 *S129A* showed stronger sensitivity than their respective single mutants. *H2B-T129A* did not
504 influence the growth of *H2A-S15A/E*.

505 (D, E) ChIP-qPCR showing γ-H2A at an inducible DSB is not affected by *H2A-S15A/E*. Cells were
506 grown in YP-raffinose overnight till log phase followed by addition of galactose to induce DSB for
507 3 hours before cross-linking the chromatin. Primer pairs used flanked the DNA sequence on both
508 left and right side at 3Kb, 7Kb and 10Kb of the DSB at *MAT* locus. Anti-H4 signal was used to
509 normalize for histone occupancy. The data represents mean of two independent biological
510 replicates. Error bars indicate the ranges between the two biological replicates.

511 (F) *H2A-S15A/E* affects the acetylation of histone H4 and H2A. Western blot analysis of yeast
512 whole cell extracts (WCE) with anti-H4ac reveals a slight reduction in H4ac and H2Aac in *H2A-*
513 *S15A* and to a lesser extent in *H2A-S15E* compared to wild type. Histone H3 was used as loading
514 control.

515 (G) *H2A-S15A/ E* show reduced H4ac signal in regions close to the DNA break site. Signal for H4ac
516 was normalized for histone occupancy on total H4 signal. ChIP-qPCR was performed as described
517 in (D), with primers flanking 150bp, 1kb, 3Kb left and 0.5Kb, 1kb, 3Kb right of DSB.
518
519 **Fig 2: H2AS15ph is locally induced upon DNA double strand break formation and spread over**
520 **several kilobases.**
521 (A) H2A-S15ph signal increased when yeast cells are treated with DNA damaging agent, MMS.
522 Western blot analysis was performed with 300ng of native chromatin purified from yeast cells
523 treated with DMSO (untreated control) and MMS. Anti-H2AS129ph was used as positive control
524 for the MMS treatment. Antibodies against histone H2B and H4 were used as loading control.
525 (B) Anti-H2AS15ph is specific for recognizing a phosphorylation mark on H2A. Western blot
526 analysis was performed with 300ng of native chromatin purified form MMS treated yeast cells
527 after incubation with or without lambda protein phosphatase (λPP). Lane with λPP treatment
528 showed a significant decrease in signal for H2A-S15ph. Histone H4 was used as loading control.
529 (C) H2AS15ph spreads on both sides of the HO endonuclease induced single DSB at *MAT* locus.
530 Signal for H2AS15ph showed enrichment after the induction of the DSB in wild type but not in
531 *H2A-S15A*. ChIP-qPCR was performed as described in Figure 1D. Fold enrichment was calculated
532 as ratio of %IP/ input normalized on total H4 for histone occupancy at indicated loci around DSB
533 at *MAT* locus to the signal at negative-control locus intergenicV.
534 (D, E) Kinetics of H2S15ph and H2AS129ph accumulation after the induction of the HO-DSB. ChIP
535 samples were analyzed after times 0, 30min, 1hr and 3hrs. Anti-H4 signal was used to normalize
536 for histone occupancy. ChIP-qPCR was performed as described in Figure 1D.

537

538 **Fig 3: Mec1^{ATR} mediates phosphorylation of H2AS15 *in vivo*.**

539 (A) Phosphorylation of H2AS129 carried out by Mec1 and Tel1. Signal for H2AS129ph at DSB in
540 *lcd1*Δ (loss of Mec1) is similar to wild type proximal to the break and much reduced distal to the
541 break. H2AS129ph signal is abolished in *lcd1*Δ*xrs2*Δ (loss of Mec1 and Tel1). The line representing
542 the signal for GAL *lcd1*Δ*xrs2*Δ is hidden behind and has similar values as uninduced/raffinose
543 samples.

544 (B) Phosphorylation of H2AS15 is mediated by Mec1 and not Tel1. Loss of H2AS15ph signal in
545 *lcd1*Δ and *lcd1*Δ*xrs2*Δ compared to WT.

546 All yeast stains used in the above experiments have *sml1*Δ background. ChIP-qPCR was
547 performed as described in Figure 1D, primer pairs flanking 1Kb left and right of DSB were also
548 used.

549

550 **Fig 4: H2AS15 regulates resection of DNA ends at DSB and Rad9^{53BP1} binding *in vitro***

551 (A) *H2A-S15E* mutant has increased DNA end resection compared to *H2A-S15A* and wild type
552 backgrounds. *H2A-S129A* is used as a positive control. ChIP-qPCR was performed as described in
553 Figure 1D with antibody against Rfa1 and primer pairs flanking 1Kb, 3Kb and 7Kb left and right of
554 DSB.

555 (B) Peptide pull-down assay with GST-tagged recombinant Rad9 and indicated H2A N-terminal
556 peptides. rRad9 binds to unmodified peptide over phosphorylated peptide. Empty GST is used as
557 negative control.

558 (C) Peptide pull-down assay as in (B) but using extracts from yeast cells treated or not with MMS
559 and expressing myc-tagged Rad9.
560 (D) Model for the role H2AS15ph in DSB repair. Mec1 phosphorylates H2AS15 in the region
561 surrounding the DSB. This phosphorylation inhibits Rad9 binding and results in increased
562 resection. H2AS15ph may function as a dynamic switch to modulate resection, phosphorylation
563 enabling resection and non-phosphorylation preventing hyper-resection.
564
565

FIGURE 1

(A)

1 15
S.cerevisiae N-SGGKGGKAGSAAKA**SQ**SRSAK
H.sapiens N--SGRGKQGGKARAKA**K**SRSSR

(B)

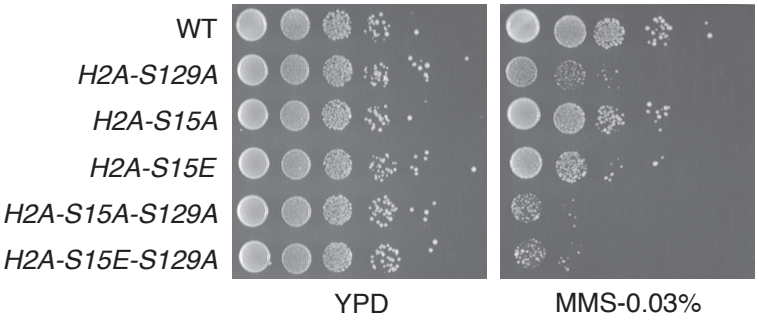

(C)

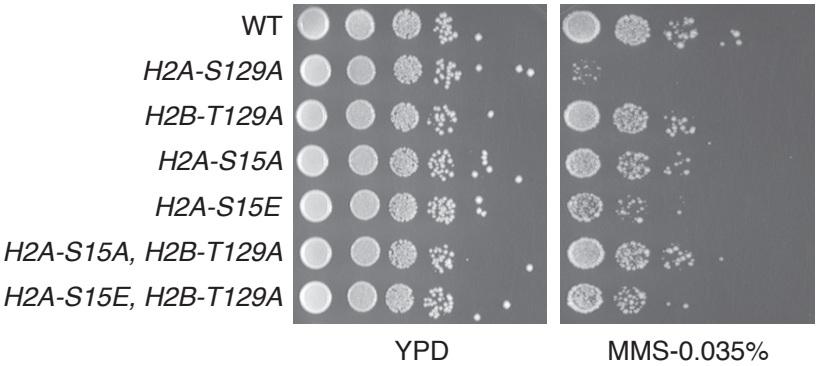

(D)

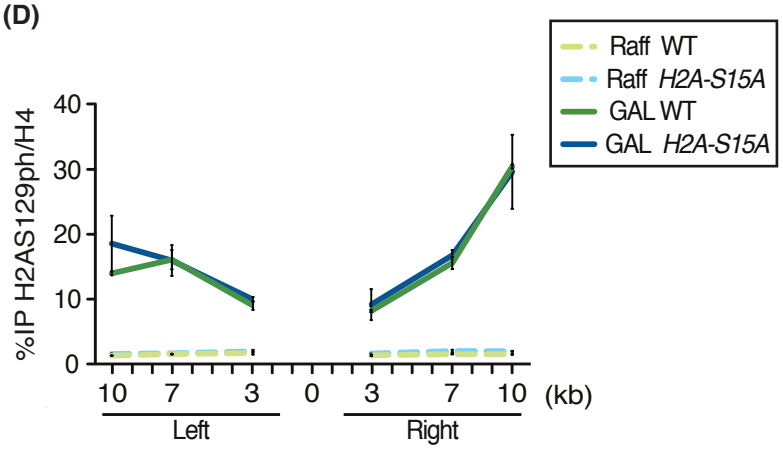

(E)

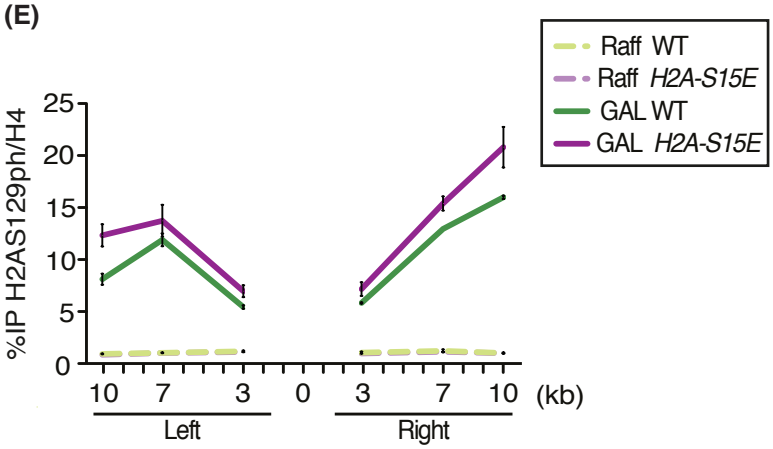

(F)

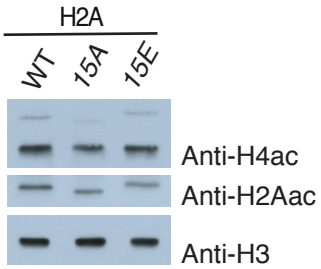

(G)

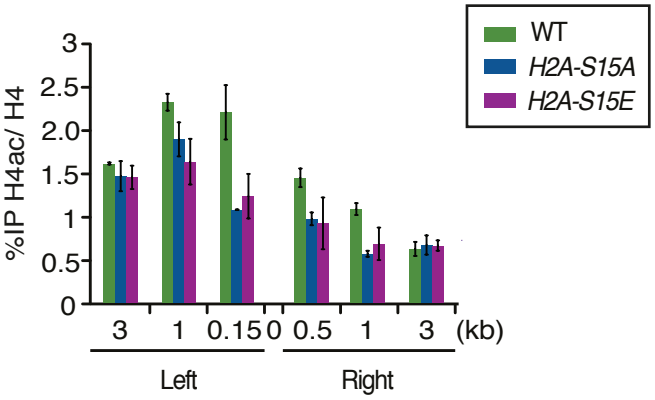

FIGURE 2

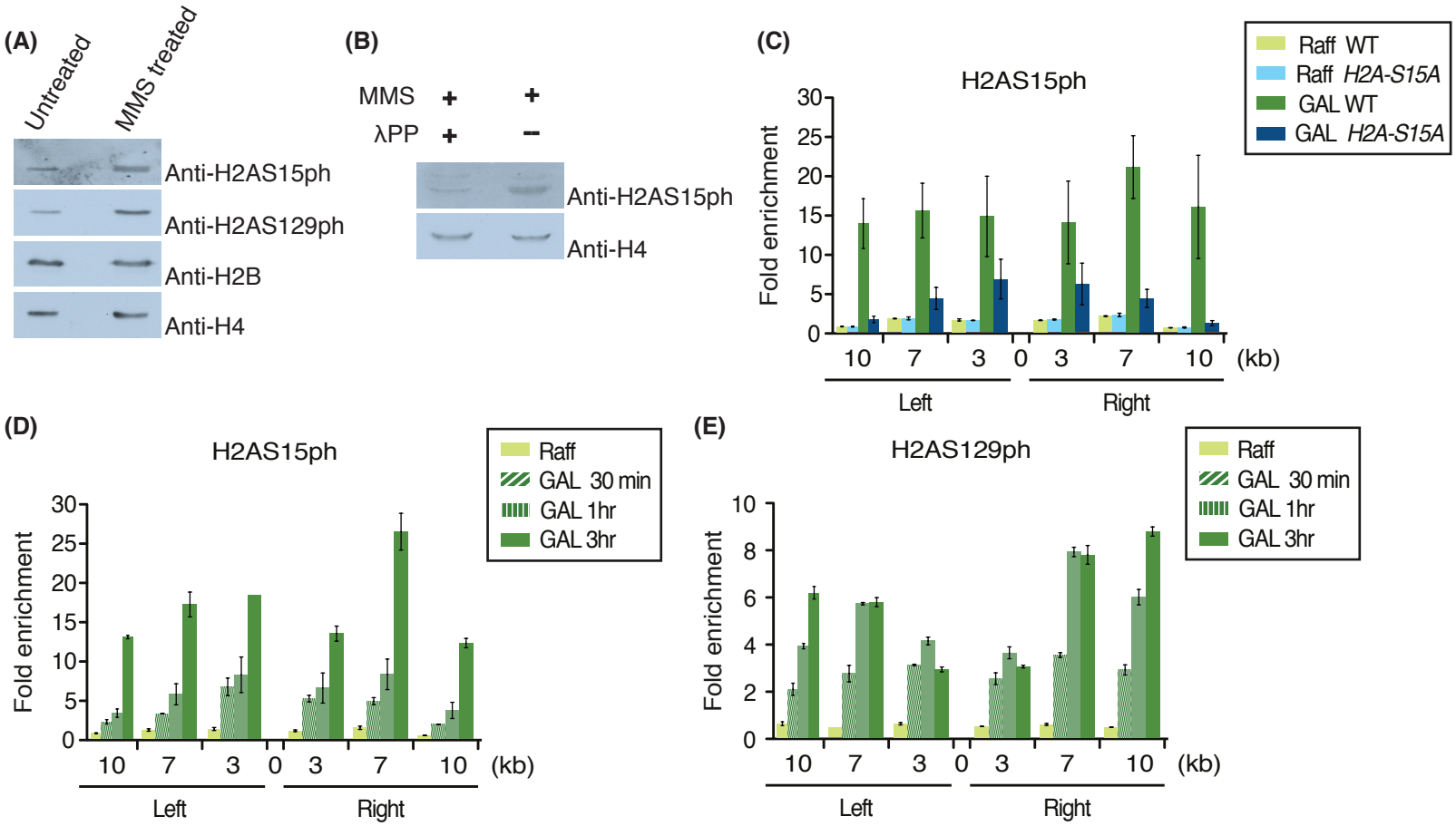
(A)
Untreated
MMS treated
Anti-H2AS15ph
Anti-H2AS129ph
Anti-H2B
Anti-H4
(B)
MMS + +
λPP + −
Anti-H2AS15ph
Anti-H4
(C)
H2AS15ph
Raff WT
Raff H2A-S15A
GAL WT
GAL H2A-S15A
Fold enrichment
0 5 10 15 20 25 30
10 7 3 0 3 7 10 (kb)
Left
Right
(D)
H2AS15ph
Raff
GAL 30 min
GAL 1hr
GAL 3hr
Fold enrichment
0 5 10 15 20 25 30
10 7 3 0 3 7 10 (kb)
Left
Right
(E)
H2AS129ph
Raff
GAL 30 min
GAL 1hr
GAL 3hr
Fold enrichment
0 2 4 6 8 10
10 7 3 0 3 7 10 (kb)
Left
Right

FIGURE 3

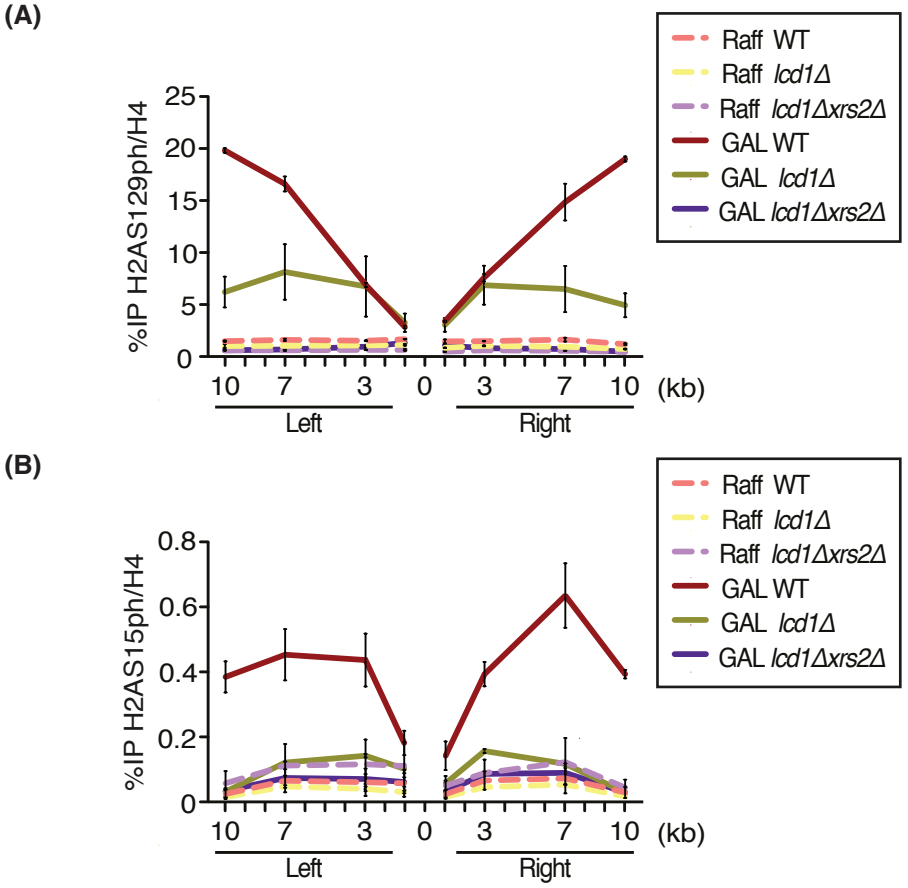
(A)
%IP H2AS129ph/H4
25
20
15
10
5
0
10
7
3
0
3
7
10
(kb)
Left
Right
Raff WT
Raff lcd1Δ
Raff lcd1Δxrs2Δ
GAL WT
GAL lcd1Δ
GAL lcd1Δxrs2Δ
(B)
%IP H2AS15ph/H4
0.8
0.6
0.4
0.2
0
10
7
3
0
3
7
10
(kb)
Left
Right
Raff WT
Raff lcd1Δ
Raff lcd1Δxrs2Δ
GAL WT
GAL lcd1Δ
GAL lcd1Δxrs2Δ

FIGURE 4

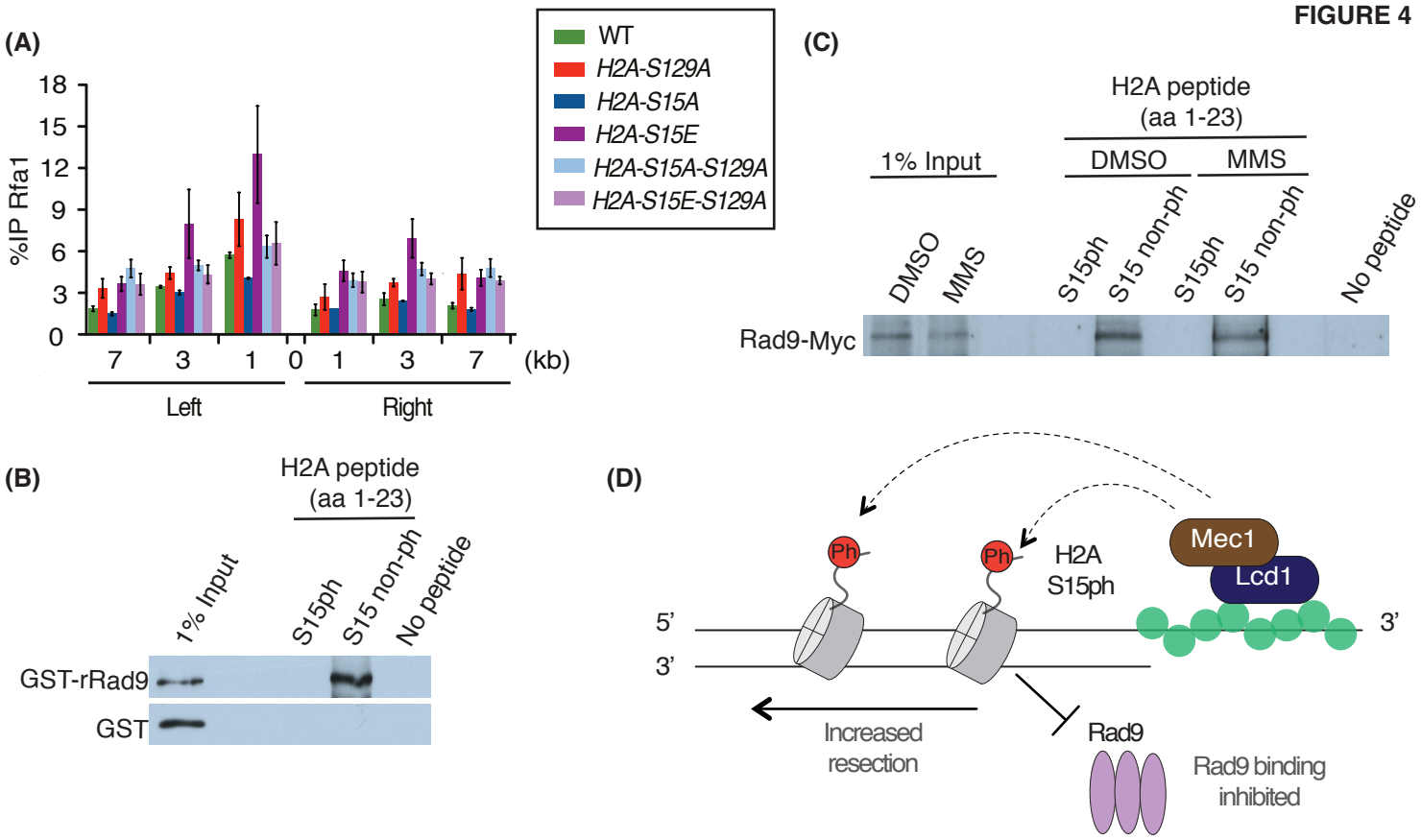
(A)
%IP Rfa1
18
15
12
9
6
3
0
7
3
1
0
1
3
7
(kb)
Left
Right
WT
H2A-S129A
H2A-S15A
H2A-S15E
H2A-S15A-S129A
H2A-S15E-S129A
(B)
H2A peptide
(aa 1-23)
1% Input
S15ph
S15 non-ph
No peptide
GST-rRad9
GST
(C)
H2A peptide
(aa 1-23)
1% Input
DMSO
MMS
DMSO
MMS
S15ph
S15 non-ph
S15ph
S15 non-ph
No peptide
Rad9-Myc
(D)
Ph
Ph
H2A
S15ph
Mec1
Lcd1
5'
3'
3'
Increased
resection
Rad9
Rad9 binding
inhibited